Supplement of Geosci. Model Dev., 17, 3949–3974, 2024
https://doi.org/10.5194/gmd-17-3949-2024-supplement

Geoscientific Model Development
Open Access
EGU

Supplement of

A revised model of global silicate weathering considering the influence of vegetation cover on erosion rate

Haoyue Zuo et al.

Correspondence to: Yonggang Liu (ygliu@pku.edu.cn) and Yongyun Hu (yyhu@pku.edu.cn)

Contents:

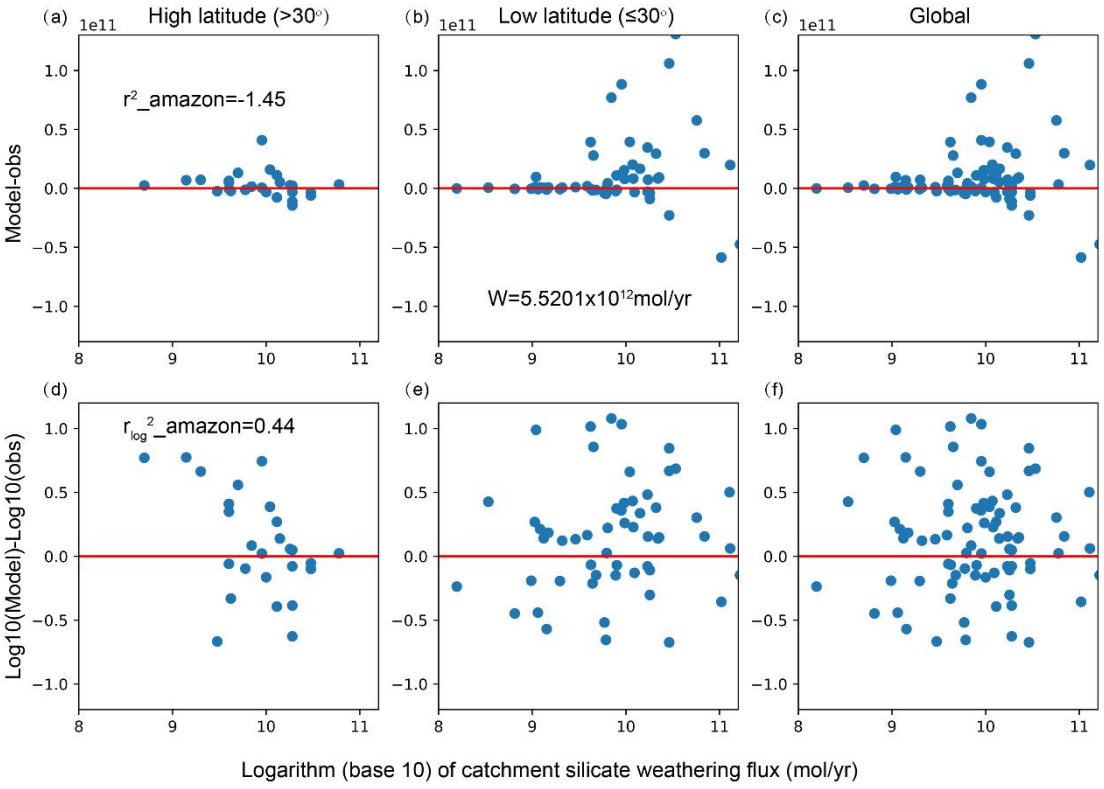

Figure S1 The difference between model calculated and observed silicate weathering fluxes for 81 large rivers over the world for model calculated with parameters provided in Maffre (2022). The upper and lower panels show model-obs and log(model)-log(obs), respectively. The left, middle and right panels show rivers in the mid- to high latitudes (more than half its river basin is >=30°), low latitudes (<30°) and over the whole globe, respectively. Calculated using the GM09 model but with model parameters in Maffre (2022). The global total weathering flux is 5.5201×10^{12} mol/yr.

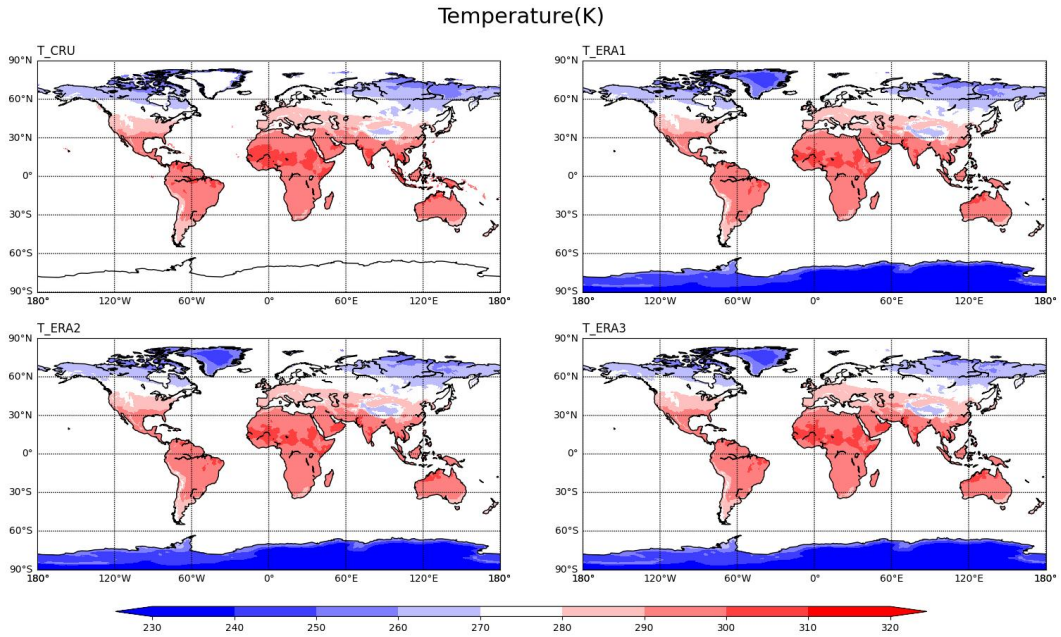

Figure S2 The distribution of temperature for the four datasets.

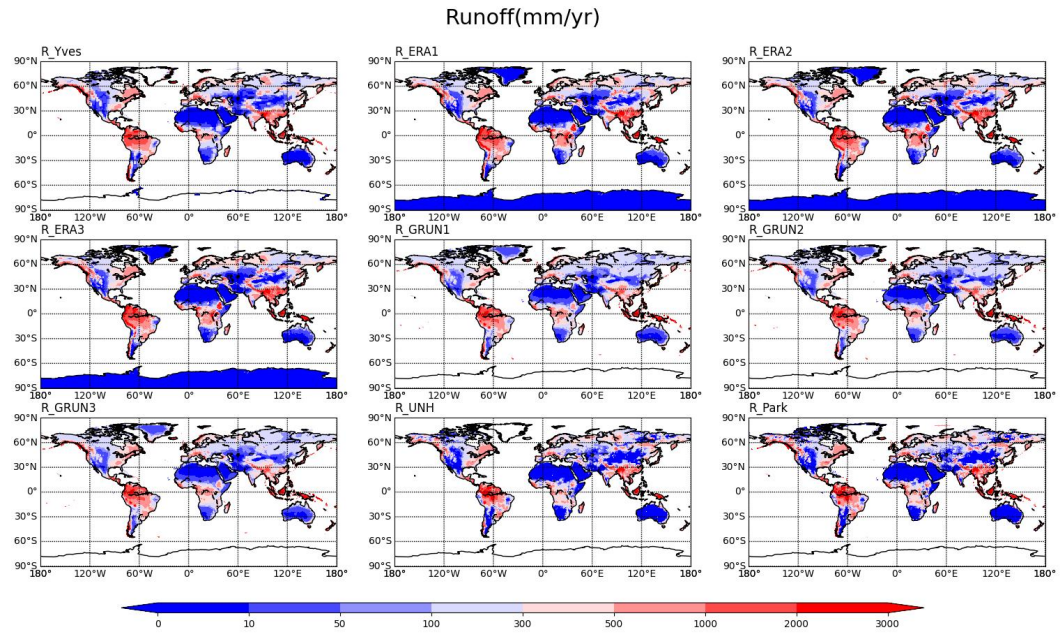

15

Figure S3 The distribution of runoff for the nine datasets.

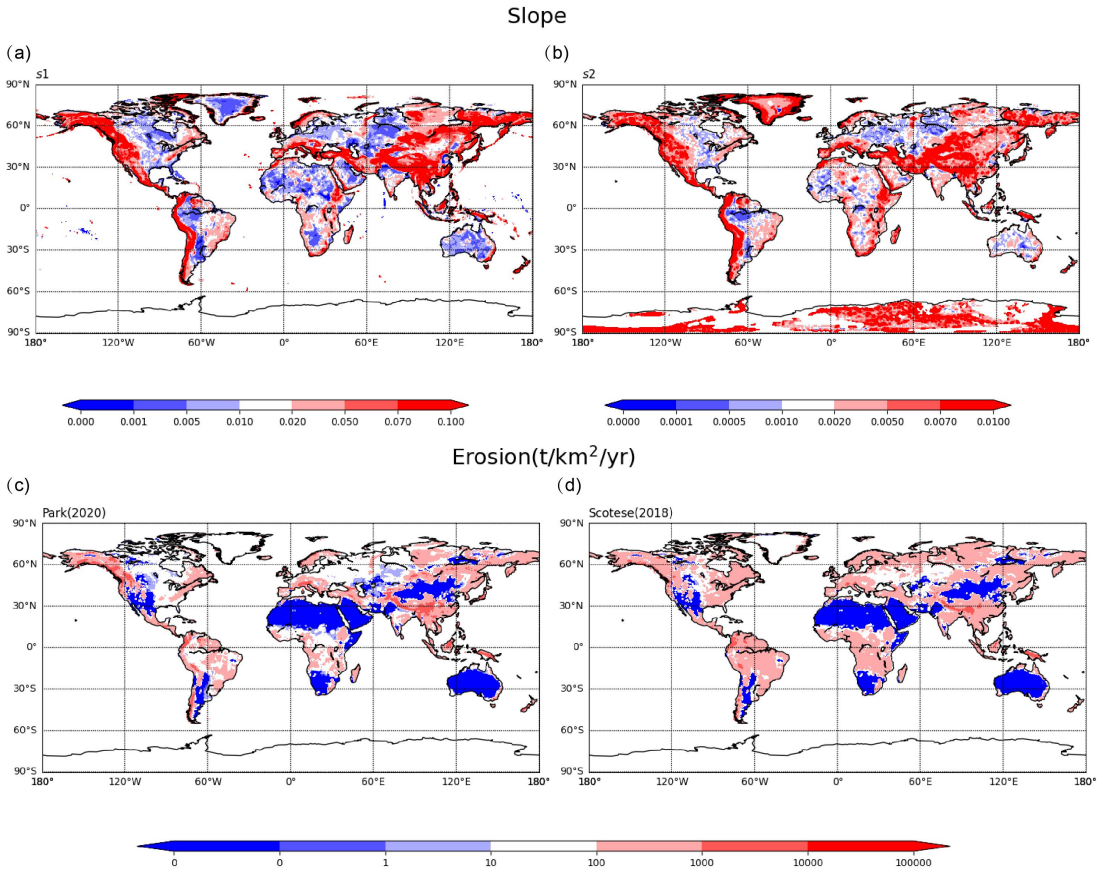

Figure S4 The distribution of slope and erosion rate for the two slope datasets with runoff from Park (2020)-UNH (R_Park).

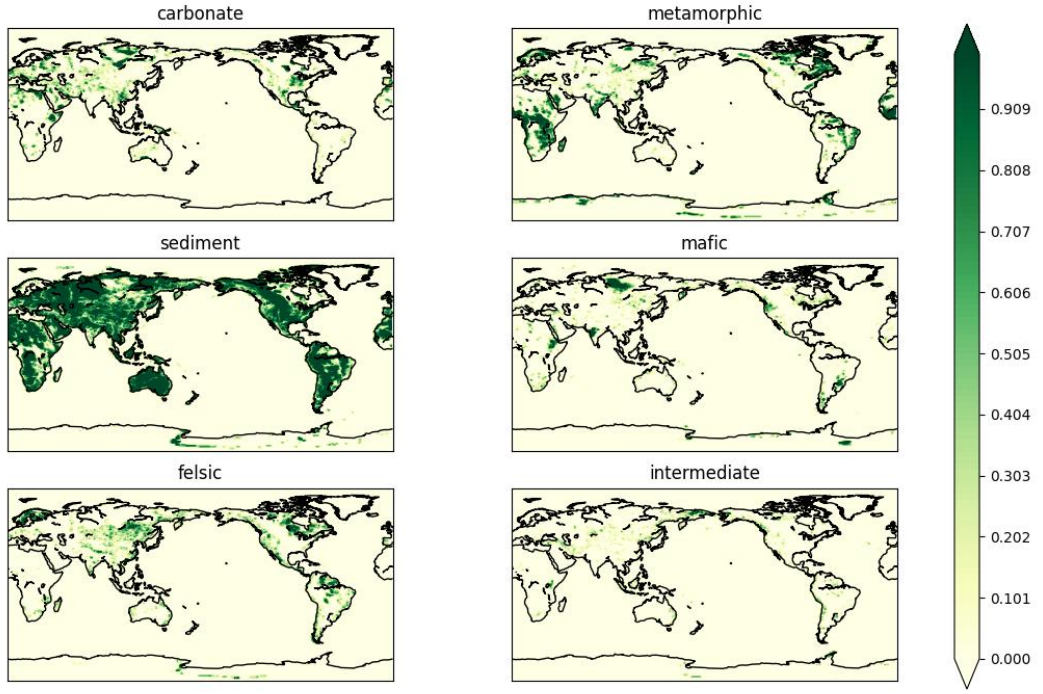

Figure S5 Distribution of lithologies modified from (Hartmann and Moosdorf, 2012).

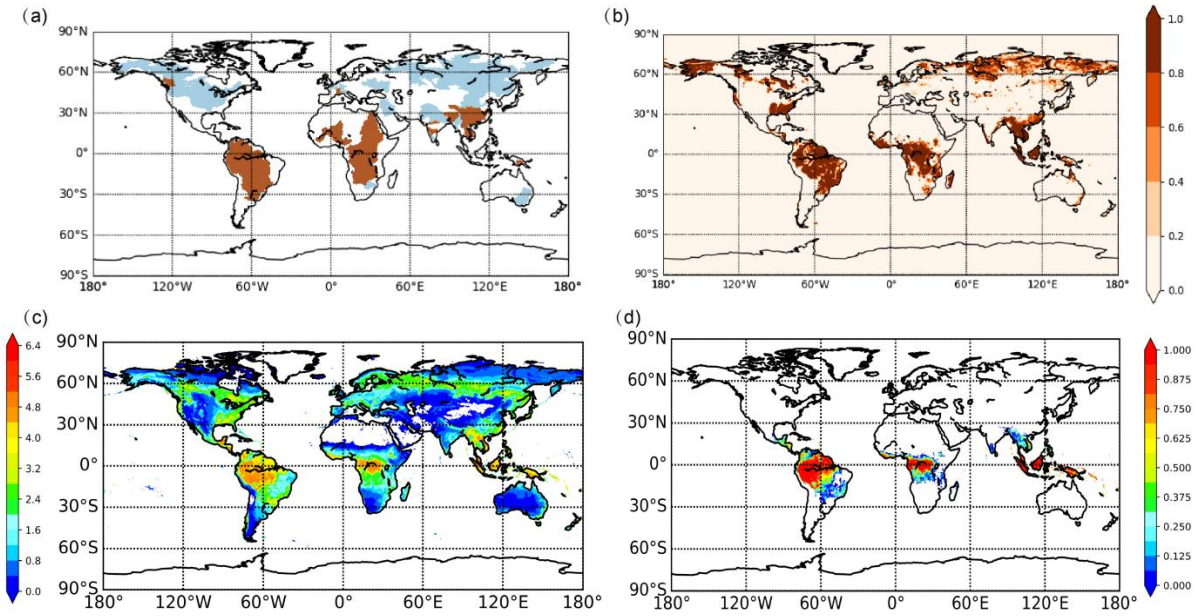

Figure S6 Distribution of overestimated river basins, leached soil, LAI, PFT. (a) is the simulation results of weathering flux for river basins, where the brown color represents overestimation and the blue color represents underestimation. The data for this figure is derived from the runoff data provided by R_Park, the topographic data from *s*2, and the adjusted erosion by TSS observation data; (b) is the distribution of leached soil from Harmonized World Soil Database, and the values represent the percentage of each grid that contains that type of soil; (c) and (d) present vegetation data from CESM (Community Earth System Model), specifically the Leaf Area Index (LAI) and tropical evergreen tree coverage, respectively.

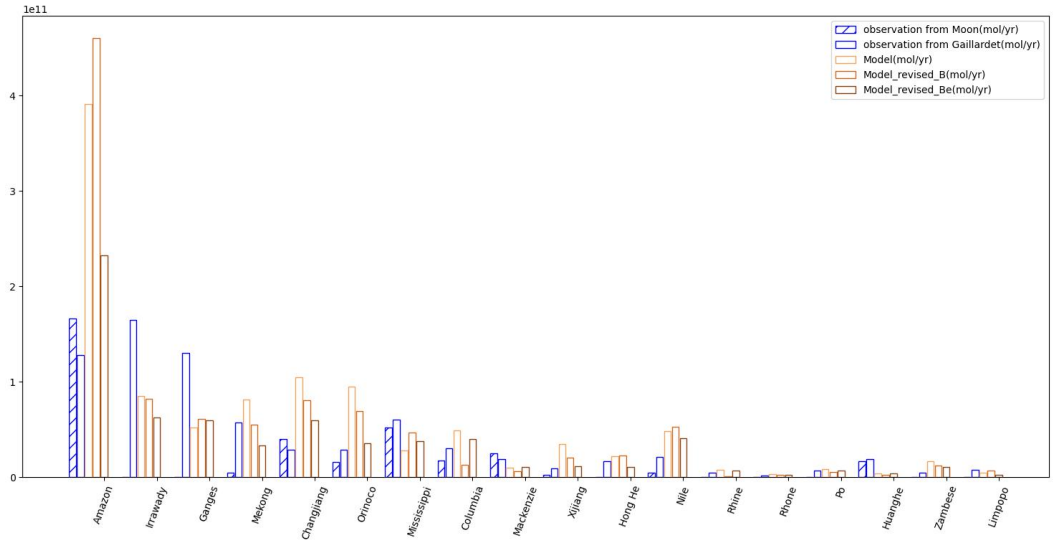

Figure S7 Histogram of silicate weathering fluxes for 18 river basins for which erosion rate from cosmogenic nuclide analysis was provided in (Wittmann et al., 2020). The blue hollow bars represent the observations from Gaillardet and bars with inclined lines represent the observations from Moon. Three different hollow bars in oranges represent the Park20 model result (T_CRU_R_Yves_*s*1_B1), revised by TSS (T_CRU_R_Yves_*s*1_BT) and revised by cosmogenic nuclide analysis erosion rate data (T_CRU_R_Yves_*s*1_Be), respectively.

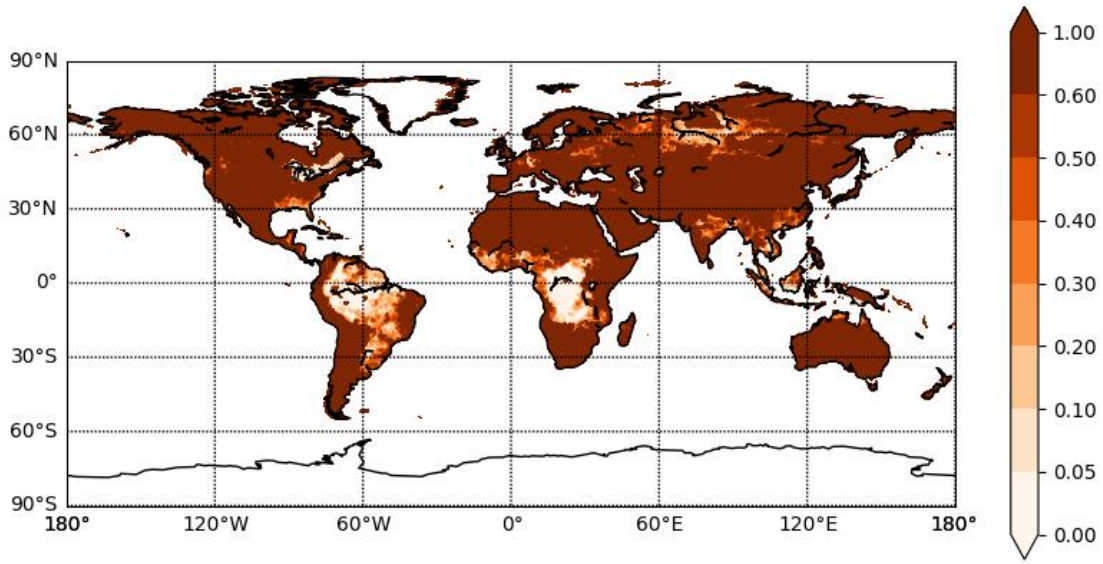

Figure S8 The concentration ratio of topsoil x_s from the Park20 model with R_Park runoff data, s2 slope data and erosion rate revised by TSS data.

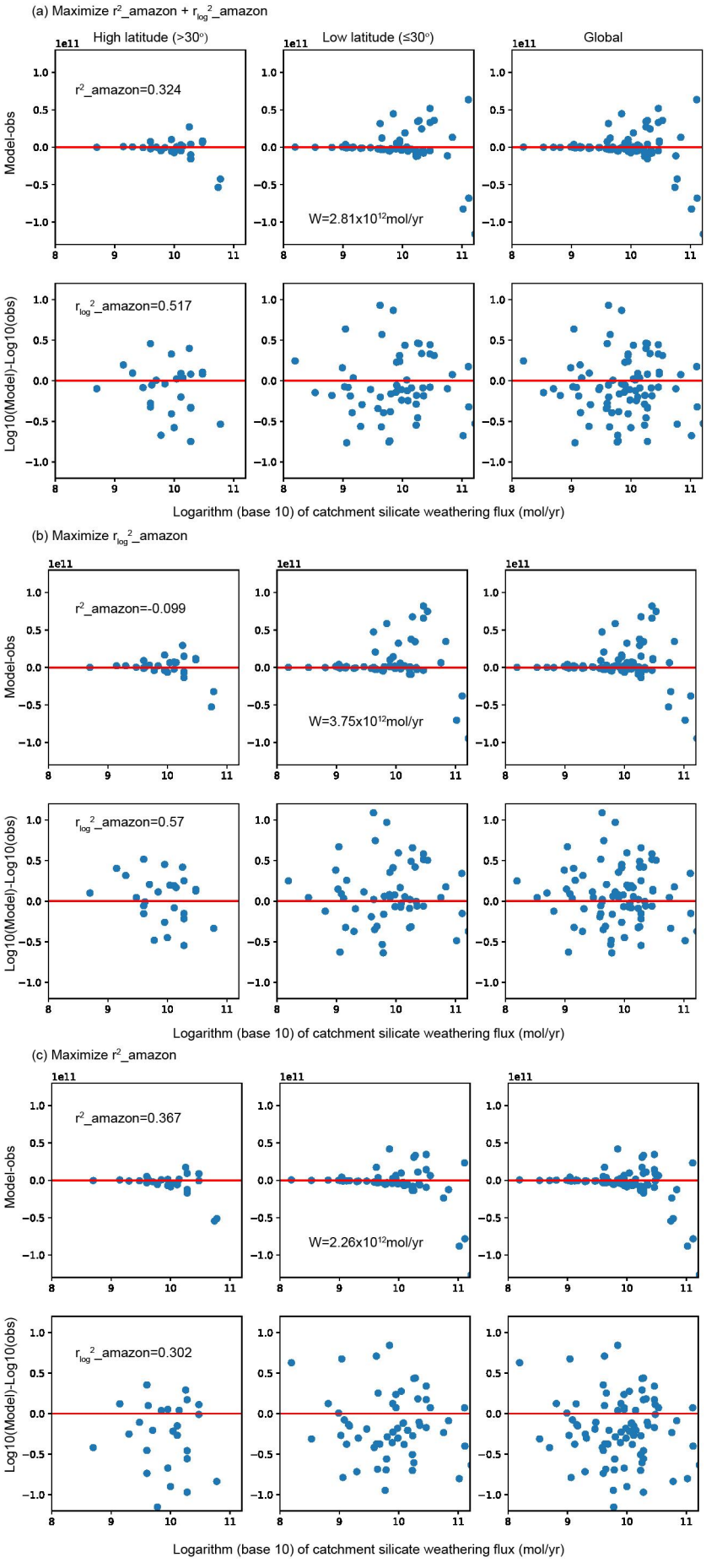
(a) Maximize r²_amazon + r_log²_amazon
High latitude (>30°)
Low latitude (≤30°)
Global
1e11
r²_amazon=0.324
W=2.81x10¹²mol/yr
r_log²_amazon=0.517
Model-obs
Log10(Model)-Log10(obs)
(b) Maximize r_log²_amazon
r²_amazon=-0.099
W=3.75x10¹²mol/yr
r_log²_amazon=0.57
(c) Maximize r²_amazon
r²_amazon=0.367
W=2.26x10¹²mol/yr
r_log²_amazon=0.302
Logarithm (base 10) of catchment silicate weathering flux (mol/yr)

Figure S9 The straight and logarithmic model-data errors at 81 river basins, respectively, when the parameter combination at the peak of light blue, orange and purple-red curve in Fig. 11b is used to calculate the weathering fluxes at each river basin.

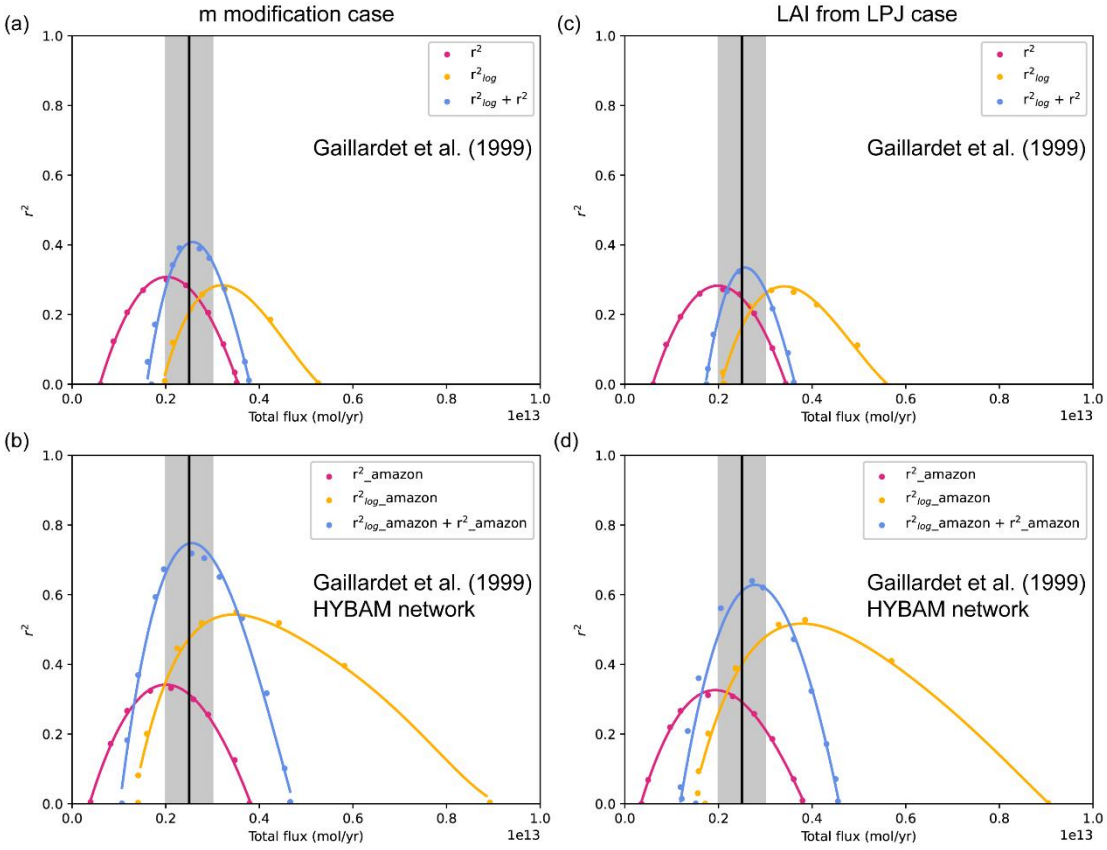

Figure S10 (a) and (b) shows the $r_{log}{}^2$ (orange) and r^2 (purple-red) and their sums (light blue) of all possible combinations of the parameters for the experiment R_Yves_*s*2_mn which changes the sensitivity of erosion rate to the runoff to be zero, and the highest R2 in this case is 0.39 and 0.72 for (a) and (b) respectively. (c) and (d) is for the case R_Yves_*s*2_LAI_old_global which uses the vegetation from LPJ model and the highest R2 in this case is 0.32 and 0.64 for (a) and (b) respectively. Both of them are the results with R_Yves runoff data. The black vertical line and grey zone in (a~d) shows the observed global total weathering flux.

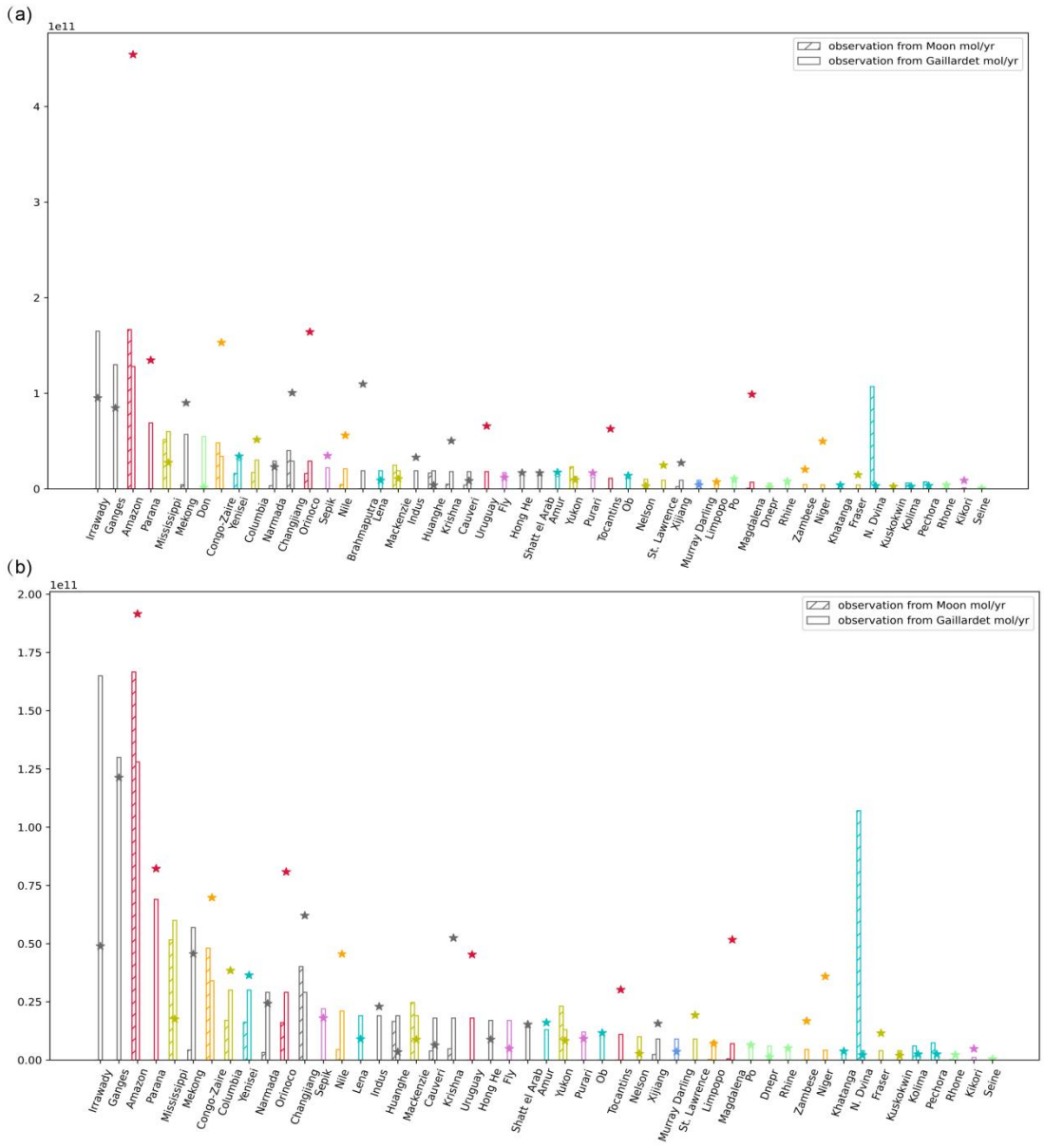

Figure S11 A comparison of the weathering flux across 51 basins as determined by the original Park20 model (a, T_CRU_R_Yves_*s*2), revised model (b, T_CRU_R_Yves_*s*2_LAI_global with new parameters) and observational data. Observational results are shown as bar charts, sourced from studies by Gaillardet and Moon. The horizontal axis is arranged in descending order based on the observed river weathering flux, and rivers that are closely ranked may have small differences between (a) and (b). The simulated weathering flux is represented by pentagrams. Distinct colors differentiate the various regions as can be seen from Fig. 3b.

Table S1. Different parameters used in different researches with the same model

Parameter	$\chi\|_{z=0}$	K	k_w	k_{rp}	σ
(Gabet and Mudd, 2009)	0.62*	0.0032	/	0.04	-0.45
(West, 2012)	0.09 (0.04-0.13)*	2.6×10^{-4} (7.6×10^{-6}-1.2×10^{-3})	7.6×10^{-2} (1.5×10^{-3}-3.0×10^{-1})	/	-0.11 (-0.34-0.13)
(Park et al., 2020)	[2500, 2000, 10317, 1521, 4759]**	5×10^{-4}	1	1×10^{-2}	-0.4
(Maffre et al., 2022)	1815**	3×10^{-4}	1.	1.2×10^{-3}	-0.11

*The mineral concentration from the first two paper is set to be the mass fraction of chemically mobile material in the bedrock (unitless). Using the density of soil and mass of Ca^{2+}+Mg^{2+}, this unitless number can be converted to the concentration.

**The mineral concentration for the last two paper is the concentration of Ca^{2+}+Mg^{2+} in unweathered bedrock (mol/m^3), and the lithology is metamorphic, sediment, mafic, felsic, intermediate.

Table S2. Detailed information of river basins that we analysis in the paper

River name	Area (10^6 km^2)	Temperature (K)	Runoff (mm/yr)	Erosion (t/km^2/yr)	Continent	Region	Ca+Mg Gaillardet (10^9mol/yr)	Ca+Mg Moon (10^9mol/yr)
Amazon	6.112	300.15	1078	204	Southern American	Low	128	166.62
Changjiang	1.808	285.15	513	267	Southern Asia	Low	29	40.09
Mississippi	2.98	283.15	195	168	Northern American	High	60	51.66
Irrawady	0.41	297.15	1185	637	Southern Asia	Low	165	
Ganges	1.05	292.15	470	530	Southern Asia	Low	130	
Yenisei	2.59	266.15	239	5	Northern Asia	High	30	16.21
Mackenzie	1.787	270.55	172	23	Northern American	High	19	24.7
St. Lawrence	1.02	278.55	330	4	Northern American	High	9	
Lena	2.49	264.15	211	8	Northern Asia	High	19	
Xijiang	0.437	294.15	831	160	Southern Asia	Low	9	2.38
Ob	2.99	272.15	135	5	Northern Asia	High	11	
Brahmaputra	0.58	288.45	879	890	Southern Asia	Low	19	
Parana	2.783	295.15	204	34	Southern American	Low	87	
Mekong	0.795	294.15	587	188	Southern Asia	Low	57	4.31
Congo-Zaire	3.698	296.75	324	12	African	Low	34	48.12
Rhine	0.224	280.45	310	12	Europe	High	5	
Yukon	0.849	268.15	236	63	Northern American	High	13	23.1
Orinoco	1.1	297.95	1032	150	Southern American	Low	29	16.06
Magdalena	0.235	297.15	1009	920	Southern American	Low	7	0.52

Columbia	0.669	281.45	353	22	Northern American	High	30	17.05
Indus	0.916	291.95	98	264	Southern Asia	High	19	
Don	0.42	280.15	69	15	Europe	High	55	
Nelson	1.132		79		Northern American	High	10	
N. Dvina	0.348	275.15	316	13	Northern Asia	High	4	107.08
Amur	1.855	272.15	185	30	Northern Asia	High	13	
Huanghe	0.752	280.95	55	1400	Southern Asia	High	19	16.55
Rhone	0.0956	286.15	565	340	Europe	High	1.4	0.27
Shatt el Arab	0.5413	294.15	85	26.3	Southern Asia	High	14	
Hong He	0.12	293.13	1025	812	Southern Asia	Low	17	
Po	0.07	286.15	667	238	Europe	High	7	0.04
Fly	0.061	298.15	2311	1500	Arc	Low	17	
Tocantins	0.757	298.85	491	117	Southern American	Low	11	
Dnepr	0.504	280.15	103	5	Europe	High	6	
Sepik	0.0787	298.37	1525	103	Arc	Low	22	
Nile	2.87	298.15	10	40	African	Low	21	4.48
Narmada	0.102	299.15	382	1174	Southern Asia	Low	29	3.27
Murray Darling	1.06	291.15	22	28	Australia	High	9	
Purari	0.0306	294.15	2749	2600	Arc	Low	13.1	
Fraser	0.22	277.15	509	92	Northern American	High	4	
Kolima	0.66	264.15	200	9	Northern Asia	High	3	6.08
Krishna	0.259	297.15	116	247	Southern Asia	Low	18	4.81
Pechora	0.324	262.15	404	19	Northern Asia	High	2	7.35
Niger	1.2	301.05	128	32	African	Low	4.2	
Uruguay	0.24	291.15	604	45	Southern American	High	1.8	
Kuskokwin	0.123	267.15	487	71	Northern American	High	4	
Cauveri	0.088	298.93	239	363	Southern Asia	Low	18	3.89
Zambese	1.33	294.15	77	15	African	Low	4.5	
Khatanga	0.364	259.15	234	5	Northern Asia	High	4.2	
Seine	0.0786	283.15	164	15	Europe	High	0.5	
Kikori	0.0132		3035		Arc	Low	1.1	
Limpopo	0.44	294.15	59	80	African	Low	8	0.27

Table S3. Erosion rate of rivers from different observations

River name	Yield (t/km^2/yr) (Milliman and Farnsworth, 2011)	Yield (t/km^2/yr) (Milliman and Syvitski, 1991)	BQART (t/km^2/yr) (Syvitski and Milliman, 2007)	TSS (t/km^2/yr) (Meybeck and Ragu, 2012)	Denudation flux from ^{10}Be (t/km^2/yr) (Wittmann et al., 2020)	Erosion rate in the paper (t/km^2/yr)
Amazon	190	190	204	196.2336	81	204
Changjiang	261	250	267	266.9027	139	267
Mississippi	121	120	124	167.7718	91	168

Irrawady	605	620	637	634.1707	379	637
Ganges	531	530	675	516.4762	491	530
Yenisei	5	5	5	5.505792		5
Mackenzie	56	23	55	23.09569	222	23
St. Lawrence	4	4	4	3.964706		4
Lena	8	5	8	6.325301		8
Xijiang	163	160	210	157.8261	68	160
Ob	5	6	5	5.404682		5
Brahmaputra	806	890		932.069		890
Parana	35	30	34	28.36939		34
Mekong	188	200	128	188.5623	88	188
Congo-Zaire		11	12	10.38399		12
Rhine	0.3	4	12		267	12
Yukon	64	71	63	67.37338		63
Orinoco	136	150	184	136.2	60	150
Magdalena	538	920	873	935.8979		920
Columbia	22	22	22	22.57698	224	22
Indus	255	260	264	272.9476		264
Don	15	18	15	5.504762		15
Nelson						
N. Dvina	12.5	13		13.59195		13
Amur	27	28	30	13.35202		30
Huanghe	1333	1400	1272	1466.622	222	1400
Rhone	615	340	591	282.4268	183	340
Shatt el Arab		26.3		194.1825		26.3
Hong He	687.5	812.5		1083.425	144	812
Po	203	280	238	220.1571	564	238
Fly	1053	1500	1235	1886.164		1500
Tocantins	117	117		99.26552		117
Dnepr		4.5	5	4.285714		5
Sepik				103.6849		103
Nile	41	40	59	40.48781	20	40
Narmada		1400	610	1174.206		1174
Murray Darling	0.9	29	3	28.29774		28
Purari	2581	2600	2355	2614.628		2600
Fraser	87	91	92	89.09091		92
Kolima	15	9	9	25.2		9
Krishna	246	260	247	246.7181		247
Pechora	14	25	19	20.21605		19
Niger	18	33	32	33.38833		32
Uruguay	27	45	28	45.9667		45
Kuskokwin	68	100	71	56.49106		71
Cauveri		363				363
Zambese	37	35	15	15.02406	10.8	15

Khatanga			4.72	5	3.983791		5
Seine	6		18	15	7.221374		15
Kikori							
Limpopo	80		80	87	74.98636	8	80

*Some rivers have had decreased sediment loads resulting from dam and irrigation like Krishna, Limpopo, Indus, Huanghe, Changjiang, Narmada, Mississippi, Xijiang, Honghe, Yenisei. Consider that silicate weathering may not respond as much quickly as the erosion rate, coupled with the fact that our observations are already relatively old, we use the previous sediment loads here.

Table S4. First set of experiment in the paper

Temp	Runoff	Slope	*B*=1	*B* tunned to TSS	*B* tunned to TSS and cosmogenic nuclide analysis
T_CRU	R_Yves	*s*1	T_CRU_R_Yves_*s*1_B1	T_CRU_R_Yves_*s*1_BT	T_CRU_R_Yves_*s*1_Be
		*s*2	T_CRU_R_Yves_*s*2_B1	T_CRU_R_Yves_*s*2_BT	T_CRU_R_Yves_*s*2_Be
	R_ERA1	*s*1	T_CRU_R_ERA1_*s*1_B1	T_CRU_R_ERA1_*s*1_BT	T_CRU_R_ERA1_*s*1_Be
		*s*2	T_CRU_R_ERA1_*s*2_B1	T_CRU_R_ERA1_*s*2_BT	T_CRU_R_ERA1_*s*2_Be
	R_ERA2	*s*1	T_CRU_R_ERA2_*s*1_B1	T_CRU_R_ERA2_*s*1_BT	T_CRU_R_ERA2_*s*1_Be
		*s*2	T_CRU_R_ERA2_*s*2_B1	T_CRU_R_ERA2_*s*2_BT	T_CRU_R_ERA2_*s*2_Be
	R_ERA3	*s*1	T_CRU_R_ERA3_*s*1_B1	T_CRU_R_ERA3_*s*1_BT	T_CRU_R_ERA3_*s*1_Be
		*s*2	T_CRU_R_ERA3_*s*2_B1	T_CRU_R_ERA3_*s*2_BT	T_CRU_R_ERA3_*s*2_Be
	R_GRUN1	*s*1	T_CRU_R_GRUN1_*s*1_B1	T_CRU_R_GRUN1_*s*1_BT	T_CRU_R_GRUN1_*s*1_Be
		*s*2	T_CRU_R_GRUN1_*s2*_B1	T_CRU_R_GRUN1_*s2*_BT	T_CRU_R_GRUN1_*s2*_Be
	R_GRUN2	*s*1	T_CRU_R_GRUN2_*s*1_B1	T_CRU_R_GRUN2_*s*1_BT	T_CRU_R_GRUN2_*s*1_Be
		*s*2	T_CRU_R_GRUN2_*s2*_B1	T_CRU_R_GRUN2_*s2*_BT	T_CRU_R_GRUN2_*s2*_Be
	R_GRUN3	*s*1	T_CRU_R_GRUN3_*s*1_B1	T_CRU_R_GRUN3_*s*1_BT	T_CRU_R_GRUN3_*s*1_Be
		*s*2	T_CRU_R_GRUN3_*s2*_B1	T_CRU_R_GRUN3_*s2*_BT	T_CRU_R_GRUN3_*s2*_Be
	R_UNH	*s*1	T_CRU_R_UNH_*s*1_B1	T_CRU_R_UNH_*s*1_BT	T_CRU_R_UNH_*s*1_Be
		*s*2	T_CRU_R_UNH_*s2*_B1	T_CRU_R_UNH_*s2*_BT	T_CRU_R_UNH_*s2*_Be
	R_Park	*s*1	T_CRU_R_Park_*s*1_B1	T_CRU_R_Park_*s*1_BT	T_CRU_R_Park_*s*1_Be
		*s*2	T_CRU_R_Park_*s2*_B1	T_CRU_R_Park_*s2*_BT	T_CRU_R_Park_*s2*_Be
T_ERA1	R_Yves	*s*1	T_ERA1_R_Yves_*s*1_B1	T_ERA1_R_Yves_*s*1_BT	T_ERA1_R_Yves_*s*1_Be
		*s*2	T_ERA1_R_Yves_*s*2_B1	T_ERA1_R_Yves_*s*2_BT	T_ERA1_R_Yves_*s*2_Be
	R_ERA1	*s*1	T_ERA1_R_ERA1_*s*1_B1	T_ERA1_R_ERA1_*s*1_BT	T_ERA1_R_ERA1_*s*1_Be
		*s*2	T_ERA1_R_ERA1_*s*2_B1	T_ERA1_R_ERA1_*s*2_BT	T_ERA1_R_ERA1_*s*2_Be
	R_ERA2	*s*1	T_ERA1_R_ERA2_*s*1_B1	T_ERA1_R_ERA2_*s*1_BT	T_ERA1_R_ERA2_*s*1_Be
		*s*2	T_ERA1_R_ERA2_*s*2_B1	T_ERA1_R_ERA2_*s*2_BT	T_ERA1_R_ERA2_*s*2_Be
	R_ERA3	*s*1	T_ERA1_R_ERA3_*s*1_B1	T_ERA1_R_ERA3_*s*1_BT	T_ERA1_R_ERA3_*s*1_Be
		*s*2	T_ERA1_R_ERA3_*s*2_B1	T_ERA1_R_ERA3_*s*2_BT	T_ERA1_R_ERA3_*s*2_Be
	R_GRUN1	*s*1	T_ERA1_R_GRUN1_*s*1_B1	T_ERA1_R_GRUN1_*s*1_BT	T_ERA1_R_GRUN1_*s*1_Be
		*s*2	T_ERA1_R_GRUN1_*s2*_B1	T_ERA1_R_GRUN1_*s2*_BT	T_ERA1_R_GRUN1_*s2*_Be
	R_GRUN2	*s*1	T_ERA1_R_GRUN2_*s*1_B1	T_ERA1_R_GRUN2_*s*1_BT	T_ERA1_R_GRUN2_*s*1_Be
		*s*2	T_ERA1_R_GRUN2_*s2*_B1	T_ERA1_R_GRUN2_*s2*_BT	T_ERA1_R_GRUN2_*s2*_Be
	R_GRUN3	*s*1	T_ERA1_R_GRUN3_*s*1_B1	T_ERA1_R_GRUN3_*s*1_BT	T_ERA1_R_GRUN3_*s*1_Be

		*s*2	T_ERA1_R_GRUN3_*s2*_B1	T_ERA1_R_GRUN3_*s2*_BT	T_ERA1_R_GRUN3_*s2*_Be
	R_UNH	*s*1	T_ERA1_R_UNH_*s*1_B1	T_ERA1_R_UNH_*s*1_BT	T_ERA1_R_UNH_*s*1_Be
		*s*2	T_ERA1_R_UNH_*s2*_B1	T_ERA1_R_UNH_*s2*_BT	T_ERA1_R_UNH_*s2*_Be
	R_Park	*s*1	T_ERA1_R_Park_*s*1_B1	T_ERA1_R_Park_*s*1_BT	T_ERA1_R_Park_*s*1_Be
		*s*2	T_ERA1_R_Park_*s2*_B1	T_ERA1_R_Park_*s2*_BT	T_ERA1_R_Park_*s2*_Be
	R_Yves	*s*1	T_ERA2_R_Yves_*s*1_B1	T_ERA2_R_Yves_*s*1_BT	T_ERA2_R_Yves_*s*1_Be
		*s*2	T_ERA2_R_Yves_*s*2_B1	T_ERA2_R_Yves_*s*2_BT	T_ERA2_R_Yves_*s*2_Be
	R_ERA1	*s*1	T_ERA2_R_ERA2_*s*1_B1	T_ERA2_R_ERA2_*s*1_BT	T_ERA2_R_ERA2_*s*1_Be
		*s*2	T_ERA2_R_ERA2_*s*2_B1	T_ERA2_R_ERA2_*s*2_BT	T_ERA2_R_ERA2_*s*2_Be
	R_ERA2	*s*1	T_ERA2_R_ERA2_*s*1_B1	T_ERA2_R_ERA2_*s*1_BT	T_ERA2_R_ERA2_*s*1_Be
		*s*2	T_ERA2_R_ERA2_*s*2_B1	T_ERA2_R_ERA2_*s*2_BT	T_ERA2_R_ERA2_*s*2_Be
	R_ERA3	*s*1	T_ERA2_R_ERA3_*s*1_B1	T_ERA2_R_ERA3_*s*1_BT	T_ERA2_R_ERA3_*s*1_Be
		*s*2	T_ERA2_R_ERA3_*s*2_B1	T_ERA2_R_ERA3_*s*2_BT	T_ERA2_R_ERA3_*s*2_Be
T_ERA2	R_GRUN1	*s*1	T_ERA2_R_GRUN1_*s*1_B1	T_ERA2_R_GRUN1_*s*1_BT	T_ERA2_R_GRUN1_*s*1_Be
		*s*2	T_ERA2_R_GRUN1_*s2*_B1	T_ERA2_R_GRUN1_*s2*_BT	T_ERA2_R_GRUN1_*s2*_Be
	R_GRUN2	*s*1	T_ERA2_R_GRUN2_*s*1_B1	T_ERA2_R_GRUN2_*s*1_BT	T_ERA2_R_GRUN2_*s*1_Be
		*s*2	T_ERA2_R_GRUN2_*s2*_B1	T_ERA2_R_GRUN2_*s2*_BT	T_ERA2_R_GRUN2_*s2*_Be
	R_GRUN3	s1	T_ERA2_R_GRUN3_*s*1_B1	T_ERA2_R_GRUN3_*s*1_BT	T_ERA2_R_GRUN3_*s*1_Be
		s2	T_ERA2_R_GRUN3_*s2*_B1	T_ERA2_R_GRUN3_*s2*_BT	T_ERA2_R_GRUN3_*s2*_Be
	R_UNH	*s*1	T_ERA2_R_UNH_*s*1_B1	T_ERA2_R_UNH_*s*1_BT	T_ERA2_R_UNH_*s*1_Be
		*s*2	T_ERA2_R_UNH_*s2*_B1	T_ERA2_R_UNH_*s2*_BT	T_ERA2_R_UNH_*s2*_Be
	R_Park	*s*1	T_ERA2_R_Park_*s*1_B1	T_ERA2_R_Park_*s*1_BT	T_ERA2_R_Park_*s*1_Be
		*s*2	T_ERA2_R_Park_*s2*_B1	T_ERA2_R_Park_*s2*_BT	T_ERA2_R_Park_*s2*_Be
	R_Yves	*s*1	T_ERA3_R_Yves_*s*1_B1	T_ERA3_R_Yves_*s*1_BT	T_ERA3_R_Yves_*s*1_Be
		*s*2	T_ERA3_R_Yves_*s*2_B1	T_ERA3_R_Yves_*s*2_BT	T_ERA3_R_Yves_*s*2_Be
	R_ERA1	*s*1	T_ERA3_R_ERA3_*s*1_B1	T_ERA3_R_ERA3_*s*1_BT	T_ERA3_R_ERA3_*s*1_Be
		*s*2	T_ERA3_R_ERA3_*s*2_B1	T_ERA3_R_ERA3_*s*2_BT	T_ERA3_R_ERA3_*s*2_Be
	R_ERA2	*s*1	T_ERA3_R_ERA3_*s*1_B1	T_ERA3_R_ERA3_*s*1_BT	T_ERA3_R_ERA3_*s*1_Be
		*s*2	T_ERA3_R_ERA3_*s*2_B1	T_ERA3_R_ERA3_*s*2_BT	T_ERA3_R_ERA3_*s*2_Be
	R_ERA3	*s*1	T_ERA3_R_ERA3_*s*1_B1	T_ERA3_R_ERA3_*s*1_BT	T_ERA3_R_ERA3_*s*1_Be
		*s*2	T_ERA3_R_ERA3_*s*2_B1	T_ERA3_R_ERA3_*s*2_BT	T_ERA3_R_ERA3_*s*2_Be
T_ERA3	R_GRUN1	*s*1	T_ERA3_R_GRUN1_*s*1_B1	T_ERA3_R_GRUN1_*s*1_BT	T_ERA3_R_GRUN1_*s*1_Be
		*s*2	T_ERA3_R_GRUN1_*s2*_B1	T_ERA3_R_GRUN1_*s2*_BT	T_ERA3_R_GRUN1_*s2*_Be
	R_GRUN2	*s*1	T_ERA3_R_GRUN2_*s*1_B1	T_ERA3_R_GRUN2_*s*1_BT	T_ERA3_R_GRUN2_*s*1_Be
		*s*2	T_ERA3_R_GRUN2_*s2*_B1	T_ERA3_R_GRUN2_*s2*_BT	T_ERA3_R_GRUN2_*s2*_Be
	R_GRUN3	*s*1	T_ERA3_R_GRUN3_*s*1_B1	T_ERA3_R_GRUN3_*s*1_BT	T_ERA3_R_GRUN3_*s*1_Be
		*s*2	T_ERA3_R_GRUN3_*s2*_B1	T_ERA3_R_GRUN3_*s2*_BT	T_ERA3_R_GRUN3_*s2*_Be
	R_UNH	*s*1	T_ERA3_R_UNH_*s*1_B1	T_ERA3_R_UNH_*s*1_BT	T_ERA3_R_UNH_*s*1_Be
		*s*2	T_ERA3_R_UNH_*s2*_B1	T_ERA3_R_UNH_*s2*_BT	T_ERA3_R_UNH_*s2*_Be
	R_Park	*s*1	T_ERA3_R_Park_*s*1_B1	T_ERA3_R_Park_*s*1_BT	T_ERA3_R_Park_*s*1_Be
		*s*2	T_ERA3_R_Park_*s2*_B1	T_ERA3_R_Park_*s2*_BT	T_ERA3_R_Park_*s2*_Be

Table S5. Parameters in k_{rp} function (in the order of a, b, c of Eq. (13) and (14))

（0.0244, 1.05, 1）	（0.015, 2.3, 1）	（0.005, 9, 1）
（0.0244, 1.05, 2）	（0.015, 2.3, 2）	（0.005, 9, 2）
（0.0244, 1.05, 4）	（0.015, 2.3, 4）	（0.005, 9, 4）
（0.0244, 1.05, 8）	（0.015, 2.3, 8）	（0.005, 9, 8）

Gabet, E. J. and Mudd, S. M.: A theoretical model coupling chemical weathering rates with denudation rates, Geology, 37, 151-154, 10.1130/G25270A.1, 2009.

Hartmann, J. and Moosdorf, N.: The new global lithological map database GLiM: A representation of rock properties at the Earth surface, Geochemistry, Geophysics, Geosystems, 13, 10.1029/2012gc004370, 2012.

Maffre, P., Godderis, Y., Pohl, A., Donnadieu, Y., Carretier, S., and Hir, G.: The complex response of continental silicate rock weathering to the colonization of the continents by vascular plants in the Devonian, American Journal of Science, 322, 461-492, 10.2475/03.2022.02, 2022.

Meybeck, M. and Ragu, A.: GEMS-GLORI world river discharge database, PANGAEA [dataset], 10.1594/PANGAEA.804574, 2012.

Milliman, J. and Farnsworth, K.: River Discharge to the Coastal Ocean – A Global Synthesis, 10.1017/CBO9780511781247, 2011.

Milliman, J. and Syvitski, J.: Geomorphic Tectonic Control of Sediment Discharge to Ocean – The Importance of Small Mountainous Rivers, Journal of Geology, 100, 525-544, 10.1086/629606, 1991.

Park, Y., Maffre, P., Godderis, Y., Macdonald, F., Anttila, E., and Swanson-Hysell, N.: Emergence of the Southeast Asian islands as a driver for Neogene cooling, Proceedings of the National Academy of Sciences of the United States of America, 117, 10.1073/pnas.2011033117, 2020.

Syvitski, J. and Milliman, J.: Geology, Geography, and Humans Battle for Dominance over the Delivery of Fluvial Sediment to the Coastal Ocean, Journal of Geology, 115, 10.1086/509246, 2007.

West, A. J.: Thickness of the chemical weathering zone and implications for erosional and climatic drivers of weathering and for carbon-cycle feedbacks, Geology, 40, 811-814, 10.1130/G33041.1, 2012.

Wittmann, H., Oelze, M., Gaillardet, J., Garzanti, E., and Blanckenburg, F.: A global rate of denudation from cosmogenic nuclides in the Earth's largest rivers, Earth-Science Reviews, 204, 103147, 10.1016/j.earscirev.2020.103147, 2020.